BRITISH JOURNAL OF HOSPITAL MEDICINE

ARTICLE

An Application of Machine-Learning-Oriented Radiomics Model in Clear Cell Renal Cell Carcinoma (ccRCC) Early Diagnosis

Gao Qiu[1], Zengzheng Dai[2], Hua Zhang[1,*]

[1]Department of Obstetrics, The First Affiliated Hospital of Chongqing Medical University, Chongqing, China
[2]Department of Ultrasound, Yubei District Hospital of Traditional Chinese Medicine, Chongqing, China
*Correspondence: ZhangHua418@outlook.com (Hua Zhang)

Abstract

Aims/Background Clear cell renal cell carcinoma (ccRCC) is a common and aggressive form of kidney cancer, where early diagnosis is crucial for improving prognosis and treatment outcomes. Radiomics, which utilizes machine learning techniques, presents a promising approach in medical imaging for the early detection and characterization of such conditions. This study aims to explore the clinical utility of a machine-learning-based radiomics model in the early diagnosis of ccRCC.

Methods Case data and abdominal computed tomography (CT) tumour images of patients with ccRCC were obtained from The Cancer Imaging Archive (TCIA) database. The dataset included 31 cases in the training set (19 males and 12 females, with an average age of 58.1 years) and 13 cases in the validation set (8 males and 5 females, with an average age of 69.6 years). The volume of interest (VOI) was manually delineated, slice by slice, along the tumour's edge in cross-sectional images of ccRCC. Radiomics features were extracted from each region of interest (ROI) using the "PyRadiomics" plug-in in 3D Slicer software (version 5.1.0, Massachusetts Institute of Technology and Brigham and Women's Hospital, Boston, MA, USA). Feature selection was performed using Least Absolute Shrinkage and Selection Operator (LASSO) regression analysis, followed by 10-fold cross-validation. The selected radiomics features were then used to construct prediction models based on two different supervised machine learning algorithms: logistic regression and random forest. The diagnostic performance of these models was evaluated using receiver operating characteristic (ROC) curves and calibration curves. Finally, clinical data were integrated with the radiomics features to enhance the prediction model.

Results A total of 44 radiomics features were ultimately selected to establish the prediction model based on the training set results. Among the two machine learning models, the logistic regression model demonstrated superior diagnostic performance. An evaluation of model establishment, considering both individual radiomics features (DifferenceVariance, JointEnergy.1, JointEntropy.2, MeanAbsoluteDeviation.7, SmallAreaHighGrayLevelEmphasis.7) and clinical data, indicated that the logistic regression model was stable and exhibited strong diagnostic performance, good calibration, and clinical applicability in patients with ccRCC. When clinical data were combined with radiomics features in the model, the area under the curve (AUC) reached 0.969, with an optimal threshold of –2.290, and sensitivity and specificity values of 89.3% and 95.2%, respectively. The calibration curve also confirmed that the logistic regression model had high calibration accuracy and greater clinical application value.

Conclusion This machine-learning-based radiomics prediction model demonstrated significant value in the early diagnosis of clear cell renal cell carcinoma (ccRCC).

Key words: tumour; clear cell renal cell carcinoma; computational models and bioinformatics; tumour diagnosis

Submitted: 7 May 2024 Revised: 10 September 2024 Accepted: 13 September 2024

How to cite this article:
Qiu G, Dai Z, Zhang H. An Application of Machine-Learning-Oriented Radiomics Model in Clear Cell Renal Cell Carcinoma (ccRCC) Early Diagnosis. Br J Hosp Med. 2024. https://doi.org/10.12968/hmed.2024.0238

Copyright: © 2024 The Author(s).

Introduction

Clear cell renal cell carcinoma (ccRCC) is the most aggressive subtype of renal cell carcinoma (RCC), associated with the poorest prognosis and highest mortality rate (Liu et al, 2022). RCC, the second most common urogenital malignancy, accounts for approximately 3% of all cancers and is one of the most prevalent primary renal malignancies (Jonasch et al, 2021; Lv et al, 2021; Siegel et al, 2020). Despite its prevalence, the pathogenesis of RCC remains inadequately understood. RCC is histologically classified into three main subtypes: ccRCC, papillary renal cell carcinoma (PRCC), and chromophobe renal cell carcinoma (ChRCC) (Frank et al, 2003; Xu et al, 2024). Globally, more than 400,000 individuals are diagnosed with RCC annually, with the majority being over 60 years old, and two-thirds of patients are male. According to Global Cancer Statistics 2018, RCC accounted for 403,262 new cases (2.2%) and a mortality rate of 1.8% (Bray et al, 2018). ccRCC is the most common subtype, representing over 80% of all RCC cases (Hsieh et al, 2017). ccRCC is frequently associated with the familial cancer syndrome Von Hippel-Lindau disease (VHL), which arises from inactivation or silencing of the normal (wild-type) allele. About 60% of sporadic ccRCC cases are also linked to *VHL* gene defects (Cohen and McGovern, 2005; Jonasch et al, 2021).

In China, there are approximately 304,000 new cases of ccRCC diagnosed annually, with around 31,000 deaths reported each year (Luo et al, 2020). Notably, 30% of patients with ccRCC present with metastatic disease at diagnosis, and 20%–30% experience relapse after partial or radical nephrectomy (Lv et al, 2021; Wolff et al, 2016). ccRCC is highly malignant, with a strong tendency for local invasion and distant metastasis. While partial or total nephrectomy remains the primary treatment for localized ccRCC, prognosis is favorable only if metastasis has not occurred. In cases of metastasis, the opportunity for curative surgery is often missed, and systemic targeted therapies or immunotherapy become the main treatment options. The survival rate for patients with advanced metastatic ccRCC remains low (Ran, 2022). Given the aggressive nature of ccRCC, it is essential to develop more sensitive, reliable, and accurate diagnostic techniques to improve tumour assessment and management (Su et al, 2015).

With the rapid advancement of medical imaging technology, radiomics is emerging as an important component of the artificial intelligence (AI) field in healthcare (Walsh et al, 2019). First introduced by Dutch scholar Lambin et al (2012), radiomics is a computer-aided diagnosis (CAD) technology. It allows medical images to be converted into high-dimensional data that can be deeply mined for valuable insights (Liu et al, 2019). Radiomics refers to the rapid extraction of quantitative features from imaging modalities such as computed tomography (CT), magnetic resonance imaging (MRI), positron emission tomography (PET), and ultrasound (US). These features are used to transform medical images into analyzable, high-dimensional data (Orlhac et al, 2021).

The rationale behind radiomics is that medical images contain information reflecting the underlying pathophysiology of diseases, and quantitative image analysis can reveal these relationships. Radiomics can be integrated with additional data

such as genetic and clinical information to aid in diagnosis, treatment evaluation, and prognosis prediction. Its main advantages include: (a) almost all cancer patients undergo digital imaging, providing a vast potential source of radiomics data; (b) radiomics offers non-invasive assessments of temporal and spatial changes in tumours; and (c) it can be routinely performed throughout treatment, allowing for continuous monitoring.

Radiomics involves extracting features from medical images and using statistical models to diagnose diseases, predict outcomes, and assess treatment efficacy. This approach supports personalized and precise treatment by guiding the selection of therapeutic strategies. The radiomics workflow includes steps such as image data acquisition, region of interest (ROI) segmentation, feature extraction, feature selection, model construction, and evaluation (Shur et al, 2021). Traditional imaging methods have not evolved to meet the growing demand for precise tumour diagnosis. These methods are often limited to qualitative and semi-quantitative assessments, which cannot detect subtle details through visual analysis alone (Chen et al, 2017). Radiomics, in contrast, reveals deeper insights from medical images, including information about disease severity, progression, or recurrence (Song et al, 2018). Compared to traditional CAD, radiomics provides more detailed and sophisticated information about tumours, particularly by identifying high-dimensional heterogeneity in images—an advantage that traditional CAD cannot match.

In recent years, radiomics has been applied to the study of various diseases, including colorectal cancer, nasopharyngeal carcinoma, glioma, lung cancer, liver tumours, and prostate cancer (Taha et al, 2021; Binczyk et al, 2021). Additionally, machine learning algorithms, particularly those utilizing supervised learning, have emerged as powerful computer-based methods. These algorithms can train on existing data to develop models capable of classifying unknown data with high accuracy. Despite the growing use of radiomics in oncology, there are currently limited reports on machine learning-based CT radiomics research focused on ccRCC.

Thus, this study aims to use CT radiomics features of ccRCC to construct a machine learning-based radiomics prediction model, with the goal of identifying early-stage ccRCC patients. This approach seeks to provide valuable insights for clinical decision-making in the management of ccRCC.

Methods

Image Data Download and Collection

The case data and abdominal CT tumour images for ccRCC were downloaded from The Cancer Imaging Archive (TCIA) database (https://tcia.at/home). TCIA provides comprehensive immunogenic analysis results based on next-generation sequencing (NGS) data for 20 solid cancers from The Cancer Genome Atlas (TCGA) and other sources. After downloading the data, "case enrollment" was performed. The enrollment process involved formulating criteria to exclude images and clinical medical records that did not meet the requirements.

Specifically, the inclusion criteria required that patients have histologically confirmed ccRCC, available preoperative abdominal CT scans in the TCIA database,

and images of adequate quality for radiomic analysis. This meant that the images needed to be free from significant motion artifacts and have sufficient resolution for proper tumour delineation. Conversely, the exclusion criteria removed patients without histologically confirmed ccRCC, those lacking available preoperative abdominal CT scans in the TCIA database, or those with CT scans of poor quality, such as those with significant motion artifacts or insufficient resolution for accurate tumour identification and analysis.

The procedure was conducted in full accordance with the principles set out in the Declaration of Helsinki. All data used in this study was sourced from TCIA, and its usage strictly adhered to TCIA's data usage policies and conditions, including restrictions on commercial use. This study was conducted in accordance with the Declaration of Helsinki. The ethics committee of The First Affiliated Hospital of Chongqing Medical University waived the requirement for informed consent for this study.

Radiomics Analysis

ROI Segmentation

ROI or volume of interest (VOI) typically refers to a specific area within medical imaging, such as a lesion, cancer, or tumour region. The segmentation of ROI/VOI is a crucial step in radiomics, requiring high repeatability and accuracy since radiomics features are primarily extracted from these segmented areas. ROI/VOI segmentation can be performed in three ways: manual segmentation, semiautomatic segmentation, and automatic segmentation. In this study, manual delineation and segmentation were carried out using the software 3D Slicer (version 5.1.0, Massachusetts Institute of Technology and Brigham and Women's Hospital, Boston, MA, USA) to create the 3D map of ROI/VOI, as illustrated in Fig. 1.

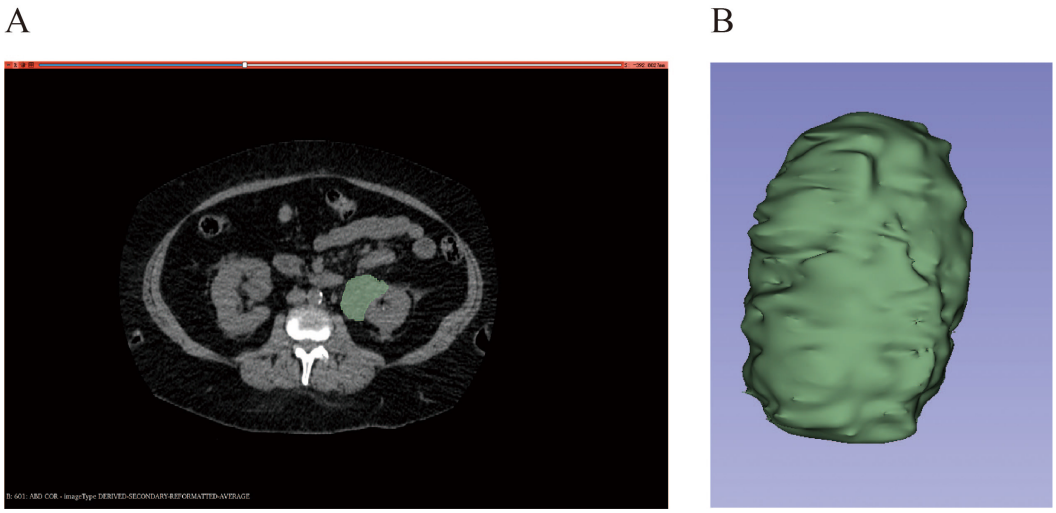

Fig. 1. Delineation of the region of interest (ROI) in renal clear cell carcinoma. (A) Drawing of abdominal computed tomography (CT) tumour contour. (B) 3D pictures presented after manual segmentation.

Feature Extraction

Shape features were used to describe the geometry of a tumour, including its shape and size. First-order statistical features analyzed the distribution of voxel intensity within the ROI. Texture features quantified the spatial distribution of gray values in the image and assessed the tumour's heterogeneity. To calculate texture features, they must first be extracted from the transformation matrix, such as the gray co-occurrence matrix. Additionally, features based on filtering or transformation involve extracting gray or texture features from the transformed image after applying transformations to the original image. Common transformation methods include wavelet transform and Gaussian filtering. In this study, radiomics features for each ROI were extracted using the "PyRadiomics" plug-in of 3D Slicer (version 5.1.0, Massachusetts Institute of Technology and Brigham and Women's Hospital, Boston, MA, USA).

Feature Selection

Feature selection is a critical step in the radiomics workflow, aiming to prevent overfitting and identify reproducible and reliable features. This process, also known as dimensionality reduction, reduces the number of features to focus on the most crucial ones. Feature selection can be categorized based on the nature of the data: supervised (labeled), unsupervised (unlabeled), and semi-supervised (partially labeled) methods (Avanzo et al, 2020).

In this study, the extracted radiomics features were standardized using classical methods and then subjected to Least Absolute Shrinkage and Selection Operator (LASSO) regression and cross-validation. The complexity adjustment in LASSO regression is controlled by the parameter λ. A larger λ imposes greater penalties on the inclusion of additional variables, ultimately resulting in a model with a more representative combination of fewer variables.

Machine Learning Model Establishment and Evaluation

Two different supervised machine learning algorithms, logistic regression and random forest, were employed to construct the prediction model. To avoid overfitting, 10-fold cross-validation was utilized. The diagnostic performance of the prediction model was assessed using the calibration curve and receiver operating characteristic (ROC) curve.

The selection of logistic regression and random forest algorithms for our study was based on several important considerations. Logistic regression, known for its simplicity and efficiency in binary classification tasks, is a fundamental tool in clinical research. Its straightforward operation facilitates easy interpretation and validation of results, which is crucial for medical applications. In contrast, the random forest algorithm, recognized for its robustness and versatility, complements logistic regression by addressing potential nonlinear relationships and interactions among features. This ensemble method enhances model prediction and reliability, particularly in complex datasets typical of radiomics research.

Our choice was guided by the nature of our research question and the specific characteristics of the data. Both algorithms have demonstrated significant success

in previous radiomics studies, particularly for handling high-dimensional data effectively. By using these two distinct yet complementary algorithms, our study aims to leverage the strengths of both approaches: the interpretability and clinical applicability of logistic regression, and the predictive power and robustness of random forest. This methodological diversity provides a comprehensive analysis, accommodating the complexities of radiomic data and improving the reliability of our findings. For model construction and evaluation, tumour stages were used as labels, with Stage I and Stage II set to 0, and Stage III and Stage IV set to 1. This binary classification was intended to differentiate between early and advanced stages for the purpose of model development.

Combined Clinical Data with Radiomics Features

Tumour/Normal, Age, Weight_kg, Weight_lb, Body Mass Index (BMI), Grade, and Path Stage_Primary_Tumour_pT were selected through univariate analysis. These seven features were combined with radiomics classification of cancer (radiomics), resulting in a total of 8 variables. Age, Weight_lb, and radiomics, identified through forward and backward stepwise screening methods, were utilized to visualize the logistic regression model in a nomogram. Finally, the calibration curve and ROC curve were employed to evaluate the model's performance.

Statistical Analysis

Data for ccRCC cases and abdominal CT images were obtained from the TCIA database (https://tcia.at/home). The ROI was manually delineated using 3D Slicer (version 5.1.0, Massachusetts Institute of Technology and Brigham and Women's Hospital, Boston, MA, USA). Radiomics features from each ROI were extracted using the "PyRadiomics" plug-in for 3D Slicer (version 5.1.0, Massachusetts Institute of Technology and Brigham and Women's Hospital, Boston, MA, USA). The machine learning prediction model was developed using the R software package version 4.2.1 (Lucent Technologies Inc., Union, NJ, USA). The calibration curve and ROC curve were utilized to predict and evaluate the model.

Statistical analysis was performed using SPSS (version 20.0, IBM, SPSS, Chicago, IL, USA). Continuous variables were assessed for normality using the Shapiro-Wilk test. Continuous variables are presented as median [minimum, maximum], with intergroup comparisons conducted using the Mann-Whitney U test. Categorical variables are presented as frequencies (percentages), and intergroup comparisons were performed using Pearson's Chi-squared test or Fisher's exact test. A p-value of <0.05 was considered statistically significant.

Result

General Patient Information

A total of 44 patients with renal clear cell carcinoma were enrolled in this study, comprising 31 patients in the training set (19 males and 12 females, with a mean age of 58.1 [range 31–90] years) and 13 patients in the validation set (8 males and 5 females, with a mean age of 69.6 [range 51–84] years). Relevant information and data from the clinical medical records were summarized, as detailed in Table 1.

Table 1. Patient characteristic.

Characteristic	Training cohort N = 31	Internal validation N = 13	Test statistic[1]	*p*-value[1]
Tumour/Normal, n (%)				<0.001
T	17 (54.8%)	0 (0%)		
TN	14 (45.2%)	13 (100%)		
Gender, n (%)			0.000	0.988
Female	12 (38.7%)	5 (38.5%)		
Male	19 (61.3%)	8 (61.5%)		
Age, Median [Min, Max]	57.00 [31.00, 90.00]	69.00 [51.00, 84.00]	–2.493	0.013
Height_cm, Median [Min, Max]	172.00 [156.00, 185.00]	170.00 [156.00, 177.00]	1.461	0.144
Height_inch, Median [Min, Max]	68.00 [62.00, 73.00]	67.00 [61.00, 70.00]	1.653	0.098
Weight_kg, Median [Min, Max]	96.00 [52.00, 167.00]	84.00 [73.00, 92.00]	2.242	0.025
Weight_lb, Median [Min, Max]	212.00 [115.00, 369.00]	185.00 [162.00, 203.00]	2.229	0.026
BMI, Median [Min, Max]	33.96 [19.00, 68.59]	28.00 [25.00, 37.00]	1.624	0.104
Race, n (%)				0.053
Unknown	14 (45.2%)	11 (84.6%)		
Asian	1 (3.2%)	0 (0%)		
White	16 (51.6%)	2 (15.4%)		
Ethnicity_self_identify, n (%)				0.760
American	1 (3.2%)	1 (7.7%)		
Caucasian	16 (51.6%)	9 (69.2%)		
Hispanic	1 (3.2%)	0 (0%)		
Indian	1 (3.2%)	0 (0%)		
Medical record does not state	3 (9.7%)	0 (0%)		
Slavonic	3 (9.7%)	2 (15.4%)		
White	6 (19.4%)	1 (7.7%)		
Tumour_site, n (%)				0.309
Lower pole	7 (22.6%)	0 (0%)		
Middle	7 (22.6%)	4 (30.8%)		
Other	5 (16.1%)	2 (15.4%)		
Upper pole	12 (38.7%)	7 (53.8%)		
Tumour_site_other, n (%)				0.167
Unknown	26 (83.8%)	11 (84.6%)		
Deep renal tumour	3 (9.7%)	0 (0%)		
Involves all three poles	0 (0%)	1 (7.7%)		
Mid lower pole	0 (0%)	1 (7.7%)		
Upper and middle pole	2 (6.5%)	0 (0%)		
Tumour_size_cm, Median [Min, Max]	4.10 [1.00, 11.00]	6.00 [4.00, 12.00]	–2.642	0.008
Tumour_focality, n (%)				0.301
Multifocal	5 (16.1%)	0 (0%)		
Unifocal	26 (83.9%)	13 (100%)		
Histologic_type, n (%)				0.082
Clear cell renal cell carcinoma	31 (100%)	11 (84.6%)		
Other	0 (0%)	2 (15.4%)		

Table 1. Continued.

Characteristic	Training cohort N = 31	Internal validation N = 13	Test statistic[1]	*p*-value[1]
Grade, n (%)				0.046
G1	1 (3.2%)	0 (0%)		
G2	23 (74.2%)	5 (38.5%)		
G3	7 (22.6%)	8 (61.5%)		
Tumour_stage_pathological, n (%)				<0.001
Stage I	22 (71.0%)	0 (0%)		
Stage II	9 (29.0%)	0 (0%)		
Stage III	0 (0%)	12 (92.3%)		
Stage IV	0 (0%)	1 (7.7%)		
AJCC_cancer_staging_edition, n (%)				
Seventh edition (2010)	31 (100%)	13 (100%)		
Sarcomatoid_features, n (%)				
Not identified	31 (100%)	13 (100%)		
Sarcomatiod_percent, n (%)				
0	31 (100%)	13 (100%)		
Path_stage_primary_tumour_pT, n (%)				<0.001
pT1a	13 (41.9%)	0 (0%)		
pT1b	11 (35.5%)	0 (0%)		
pT2a	6 (19.4%)	0 (0%)		
pT2b	1 (3.2%)	1 (7.7%)		
pT3	0 (0%)	2 (15.4%)		
pT3a	0 (0%)	10 (76.9%)		
Path_stage_reg_lymph_nodes_pN, n (%)				0.082
pN1	0 (0%)	2 (15.4%)		
pNX	31 (100%)	11 (84.6%)		
Path_stage_dist_mets_pM, n (%)			0.943	0.332
No pathologic evidence of distant metastasis	11 (35.5%)	2 (15.4%)		
Staging incomplete	20 (64.5%)	11 (84.6%)		
Clin_stage_dist_mets_cM, n (%)				0.739
cM0	3 (9.7%)	2 (15.4%)		
cM1	1 (3.2%)	0 (0%)		
Staging incomplete	27 (87.1%)	11 (84.6%)		
Serum_calcium, n (%)				0.065
Low	5 (16.1%)	0 (0%)		
Normal	2 (6.5 %)	2 (15.4%)		
Not evaluated	11 (35.5%)	9 (69.2%)		
Unknown	13 (41.9%)	2 (15.4%)		
Hemoglobin, n (%)				>0.999
Elevated	1 (3.2%)	0 (0%)		
Low	17 (54.8%)	8 (61.5%)		
Normal	7 (22.6%)	3 (23.1%)		
Unknown	6 (19.4%)	2 (15.4%)		

Table 1. Continued.

Characteristic	Training cohort	Internal validation	Test statistic[1]	*p*-value[1]
	N = 31	N = 13		
Platelets, n (%)				>0.999
Normal	24 (77.4%)	11 (84.6%)		
Not evaluated	1 (3.2%)	0 (0%)		
Unknown	6 (19.4%)	2 (15.4%)		
White_cell_count, n (%)				0.805
Elevated	3 (9.7%)	0 (0%)		
Low	1 (3.2%)	0 (0%)		
Normal	21 (68.7%)	11 (84.6%)		
Unknown	6 (19.4%)	2 (15.4%)		
History_of_cancer, n (%)	0 (0%)	3 (23%)		0.022
History_of_treatment, n (%)				0.022
Unknown	31 (100%)	10 (76.9%)		
Surgery	0 (0%)	3 (23.1%)		
Vital_status, n (%)				>0.999
Deceased	1 (3.2%)	0 (0%)		
Living	30 (96.8%)	13 (100%)		

[1]Pearson's Chi-squared test; Wilcoxon rank sum test; Fisher's exact test.
BMI, Body Mass Index; AJCC, American Joint Committee on Cancer; pT, Pathological Stage of Primary Tumour; pN, Pathological Stage of Regional Lymph Nodes; pM, Pathological Stage of Distant Metastasis; cM, Clinical Stage of Distant Metastasis.

Feature Extraction from CT Images of ccRCC

The "PyRadiomics" plug-in for 3D Slicer software (version 5.1.0, Massachusetts Institute of Technology and Brigham and Women's Hospital, Boston, MA, USA) automatically extracted 851 radiomics features from each ROI. These features include first-order statistical features (such as energy, entropy, mean, standard deviation, maximum value, etc.), shape-based and size-based morphological features (including maximum 3D diameter, volume, surface area, etc.), texture features (such as gray level co-occurrence matrix (GLCM) and gray level run-length matrix (GLRLM)), and wavelet transform-based features.

Feature Selection of CT Images of ccRCC

As shown in Fig. 2, as the regularization coefficient λ increases, the coefficients of each feature gradually approach 0, with some features rapidly reaching 0. Different ranges of λ correspond to varying numbers of features, and the most suitable λ value determines the selected features. To verify the stability of the LASSO results, 10-fold cross-validation was conducted, ultimately identifying 11 important features.

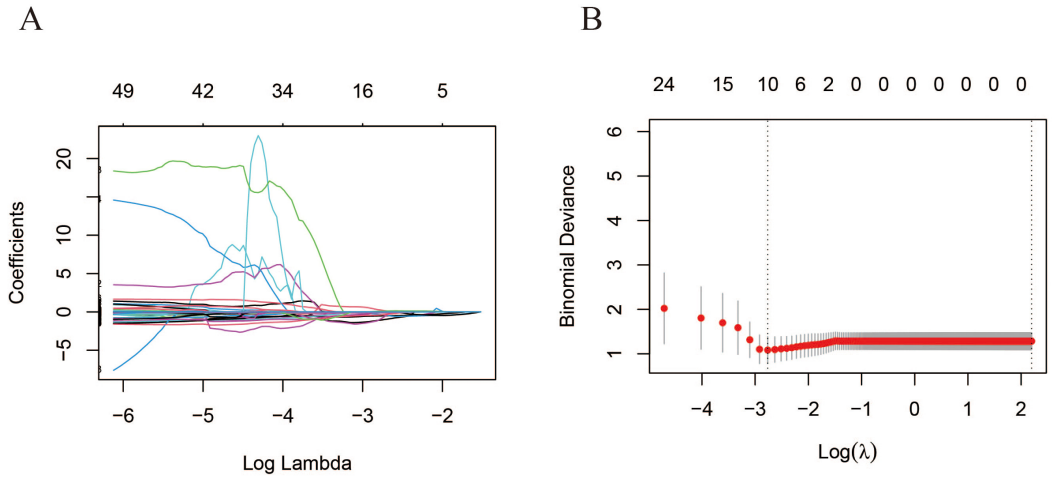

Fig. 2. Minimum absolute contraction and selection operator regression analysis for screening radiomics features. (A) Radiomics feature coefficient distribution map. (B) Plot of binomial deviation as a function of parameter λ.

Model Construction and Evaluation

Logistic Regression Model Construction and Evaluation

Before constructing the logistic regression model, the forward-to-backward stepwise regression method was employed to further identify important features (Table 2). Stepwise regression reduces multicollinearity by eliminating variables that are less significant and highly correlated with other variables. Variables were introduced into the model one by one, with an F test performed on each explanatory variable. The *t*-test was then conducted on the variables that had been selected. If an originally introduced explanatory variable became non-significant due to the introduction of subsequent variables, it was removed to ensure that only significant variables were retained in the regression equation before each new variable was added. This process was repeated until no more significant explanatory variables could be added and no insignificant variables could be removed, ensuring that the final set of explanatory variables was optimal. Ultimately, 5 radiomics features were selected to construct the prediction model: JointEnergy.1, JointEntropy.2, DifferenceVariance, MeanAbsoluteDeviation.7, and SmallAreaHighGrayLevelEmphasis.7. The non-zero coefficients of these features, determined through the forward and backward stepwise regression method, were used to create radiomics labels for the LASSO-logistic model, as illustrated in the nomogram (Fig. 3).

The calibration curve and ROC curve were used to evaluate the performance of the logistic regression prediction model. The calibration curve results demonstrated that the logistic regression model had good calibration in both the training set and the validation set, with no significant deviation between the predicted curve and the ideal curve. The Hosmer-Lemeshow test showed that the logistic regression model was not statistically significant in the training set and validation set (p = 0.05), indicating that the predicted probabilities were well aligned with the actual probabilities, and the calibration curve was not deviated from the fit, as shown in Fig. 4A,B. The ROC curve further indicated that the logistic regression model

Table 2. Forward and backward method for screening feature vectors.

	Estimate	Std. error	z value	Pr (>|z|)
(Intercept)	–4.64062	2.347688	–1.97668	0.048078
Difference variance	–1.81066	1.557942	–1.16221	0.04515
JointEnergy.1	–34.0186	17.78523	–1.91275	0.035781
JointEntropy.2	2.529273	1.006815	2.512153	0.012
MeanAbsoluteDeviation.7	–0.58615	0.304806	–1.92303	0.044476
SmallAreaHighGrayLevelEmphasis.7	0.26949	0.178397	1.510625	0.030884

Note: Pr <0.05 was selected as the final feature.
Pr, Probability.

exhibited high diagnostic efficacy and stability in both the training and validation sets, with an area under the curve (AUC) of 0.839, an optimal threshold of 0.090, a specificity of 96.8%, and a sensitivity of 61.5%, as shown in Fig. 4C.

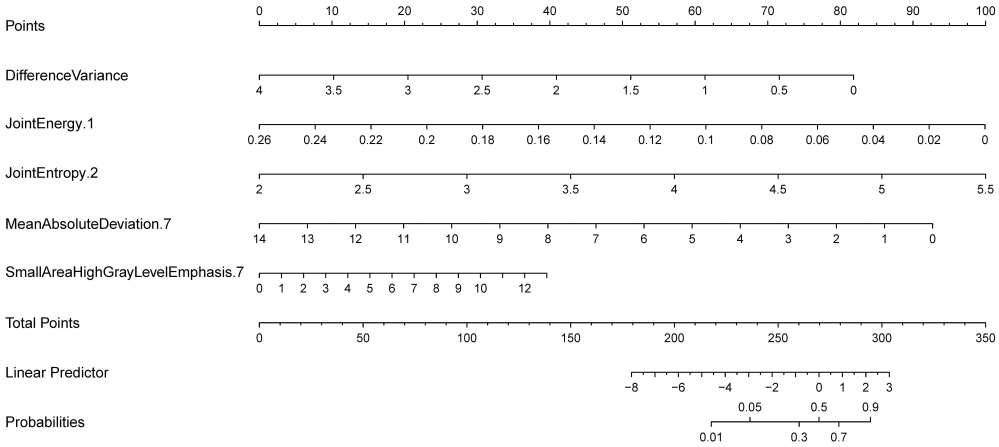

Fig. 3. Nomogram of the logistic regression prediction model.

Random Forest Model Construction and Evaluation

First, the training and test sets were divided in a 7:3 ratio for the construction of the random forest model. The model was then established (Fig. 5A) to evaluate the relationship between model error and the decision tree. After establishing the decision tree model, the saliency of each feature was assessed. In terms of the importance of radiomics features in the model, features positioned closer to the upper right corner were considered more important (Fig. 5B). The results indicated that the radiomics features Percentile.4, Percentile.5, and SizeZoneNonUniformity.6 were particularly significant.

After the model was established, the prediction accuracy was evaluated by the ROC curve. Each point on the ROC curve reflected the receptivity to the same signal stimulus. ROC curve showed that the random forest model had a high diagnostic efficacy and stability in the training and validation sets, with an AUC of 0.913, an optimal threshold of 1.500, a 90.3% specificity, and a 92.3% sensitivity, as shown in Fig. 6.

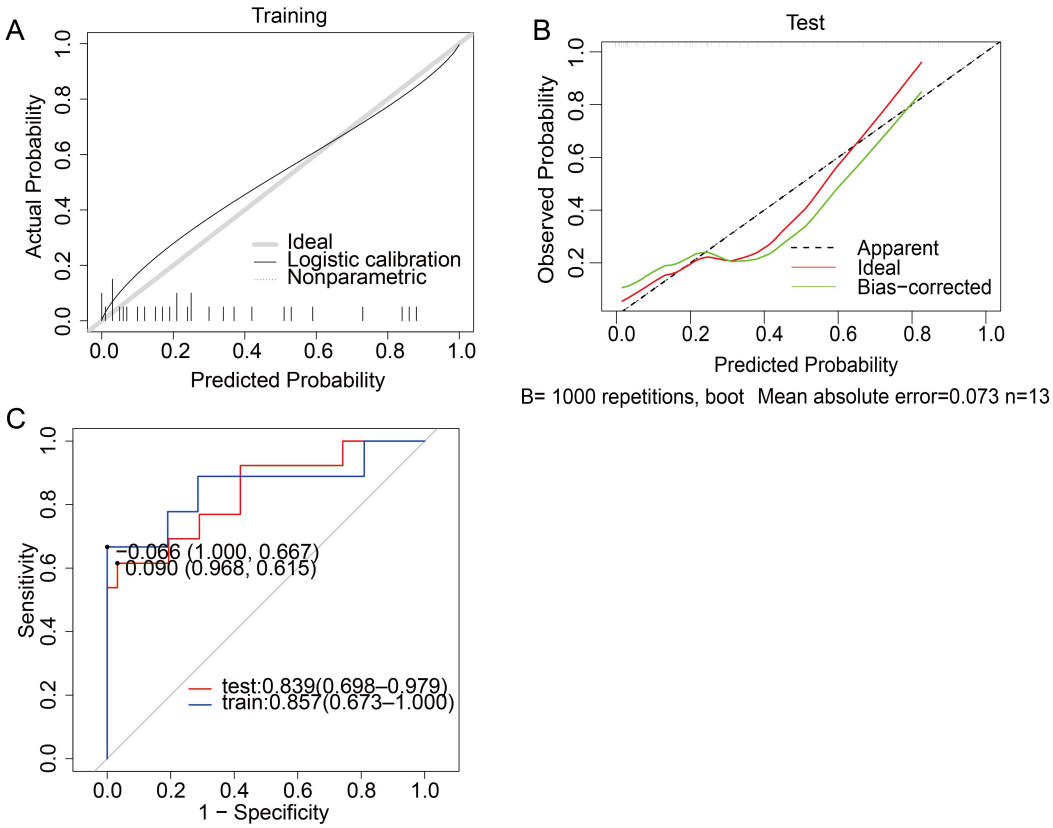

Fig. 4. Calibration curve and receiver operating characteristic (ROC) curve of a logistic regression model. (A) Calibration curve of the training set. (B) Calibration curve of the test set. The horizontal axis represents predicted probability, while the vertical axis represents probability, which ranges from 0 to 1. Apparent: line of reference; The predicted value is equal to the actual value; Ideal: The theoretical curve predicted by the model; Bias-corrected: active curve. (C) Area under the curve (AUC) is the area under the ROC curve. The maximum value is 1. The point in the upper left corner is the optimal threshold; specificity and sensitivity are listed in parentheses.

Clinical Data Combined with Radiomics Features

Clinical features (Tumour/Normal, Age, Weight_kg, Weight_lb, BMI, Grade, and Path Stage_Primary_Tumour_pT) were combined with radiomics for cancer classification, resulting in a total of 8 variables. Through forward and backward stepwise selection, three features (Age, Weight_lb, and radiomics) were identified, as shown in Fig. 7.

The calibration curve and ROC curve were used to evaluate model performance (Fig. 8). The results indicated that the logistic regression model demonstrated high and stable diagnostic performance in identifying patients with renal clear cell carcinoma based on clinical data and radiomics features. The calibration curve and Hosmer-Lemeshow goodness-of-fit test confirmed that the predicted probabilities were well aligned with the actual probabilities. The model achieved an AUC of 0.969, with an optimal threshold of –2.290, a sensitivity of 89.3%, and a specificity of 95.2%.

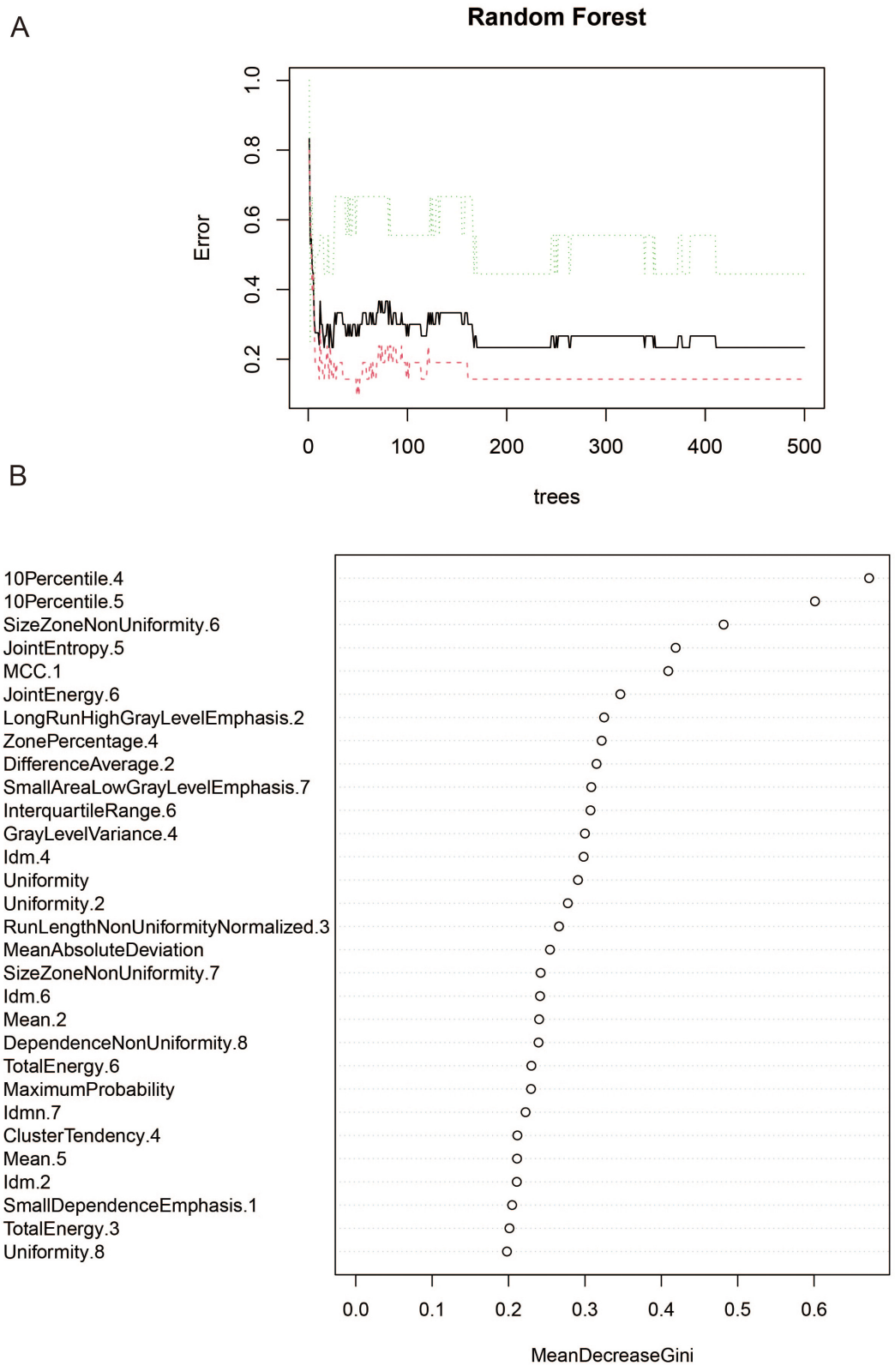

Fig. 5. Random forest prediction model. (A) Random forest model construction and error analysis. The horizontal axis represents the number of decision trees. The vertical axis represents the model error. (B) Feature importance ranking for the random forest model. The horizontal axis represents the feature importance. The vertical axis represents the feature name.

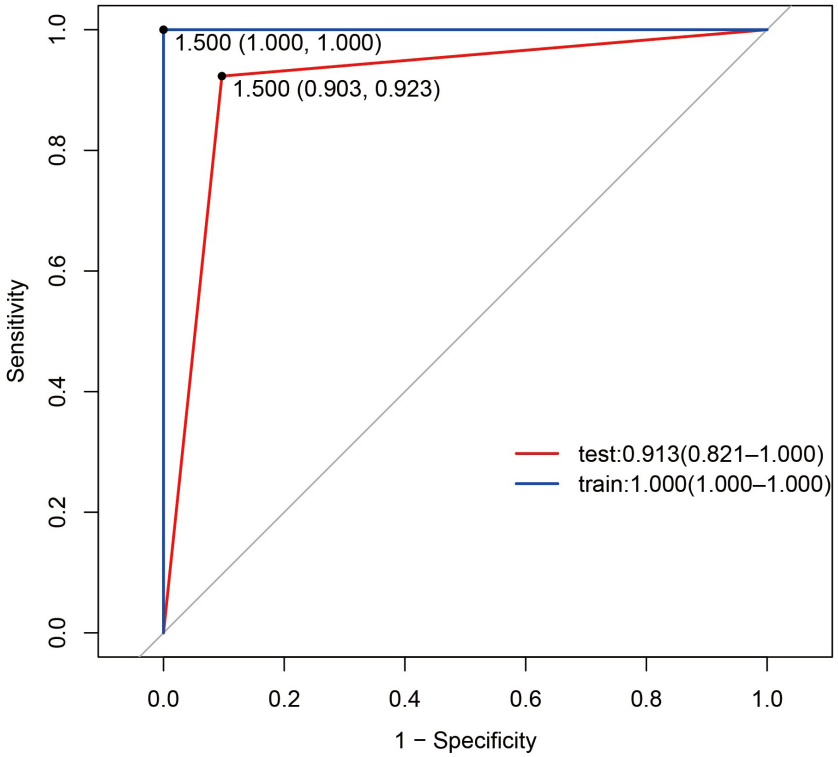

Fig. 6. ROC curve of the random forest prediction model. The horizontal axis represents 1-specificity, while the vertical axis represents sensitivity. The AUC is the area under the ROC curve, with a larger AUC indicating a better model performance. The maximum possible AUC value is 1. The blue shaded area in the figure represents the AUC corresponding to the blue curve. The point in the upper left corner of the plot indicates the optimal threshold, with specificity and sensitivity values listed in parentheses.

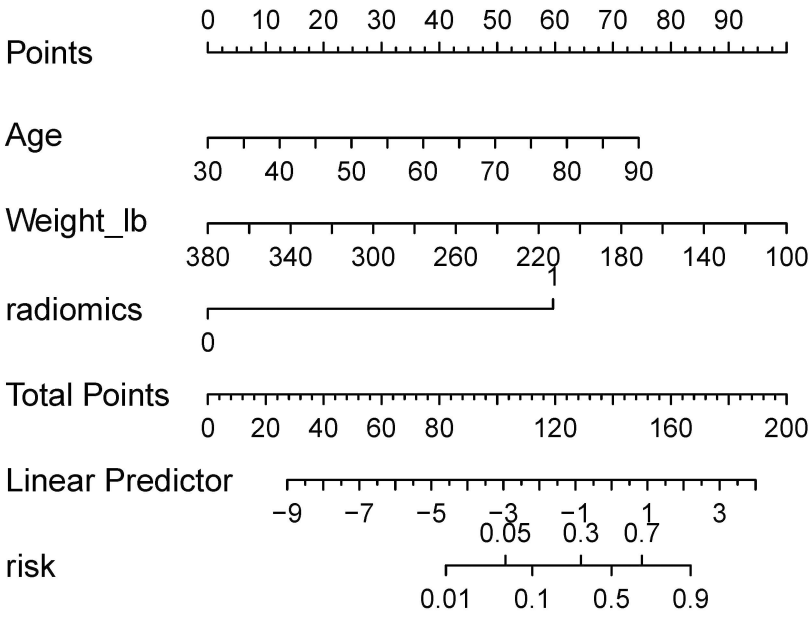

Fig. 7. Nomogram of a logistic regression prediction model for clinical data combined with radiomics features.

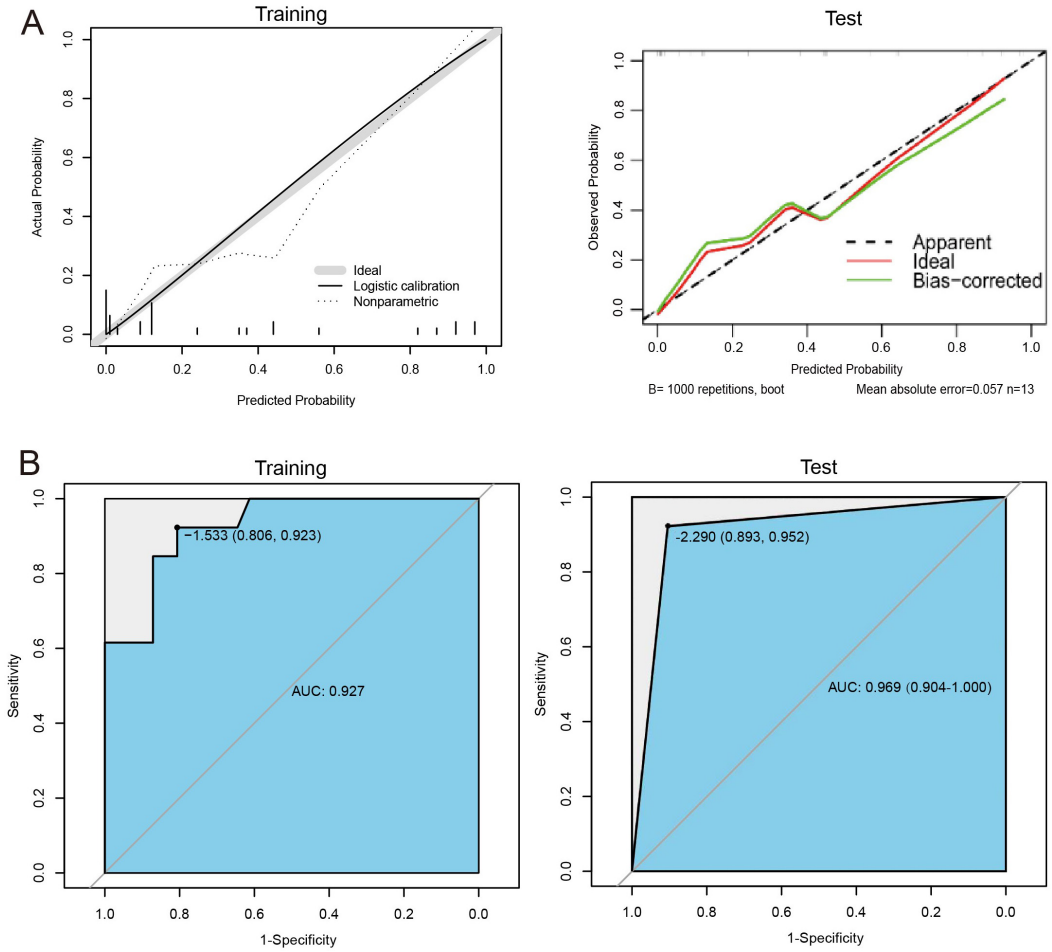

Fig. 8. Calibration curve and ROC curve. (A) The horizontal axis represents the predicted probability, while the vertical axis represents probability, which ranges from 0 to 1. Apparent: line of reference. The predicted value is equal to the actual value; Ideal: the theoretical curve predicted by the model. Bias-corrected: active curve. (B) The horizontal axis represents 1-specificity, while the vertical axis represents sensitivity. The larger the AUC is, the better the model is. The maximum value is 1. The point in the upper left corner is the optimal threshold. specificity and sensitivity are listed in parentheses.

Discussion

Surgery is considered the optimal treatment for early-stage ccRCC, as this malignancy is resistant to both chemotherapy and radiotherapy. While targeted therapies are available, their efficacy is limited. Current research in renal carcinoma focuses on enhancing early diagnosis rates and extending patient lifespans. Radiomics, combined with CAD technology, offers a promising approach for the early diagnosis and precise treatment of ccRCC. In our study, we developed two machine learning-based radiomics prediction models using CT radiomics features: logistic regression and random forest. Evaluation of these models revealed that the logistic regression model exhibited strong diagnostic efficiency, calibration, and clinical applicability when integrating clinical data with radiomics features.

Radiomics combines radiology with omics fields such as genomics and proteomics, enhancing our understanding of various medical conditions. It involves

extracting quantitative features from medical images that are often difficult to observe visually. AI encompasses algorithms that make predictions based on patterns learned from provided data. Recently, imaging techniques have been applied to early diagnosis, treatment, and prognosis, particularly in tumour diagnosis (Xu et al, 2020).

One study investigated whether CT imaging features could predict coagulation necrosis (CN) in renal clear cell carcinomas before surgery. Radiomics features offer a potential noninvasive tool for preoperative prediction of CN in ccRCC. Additionally, radiomic analysis of MRI was evaluated to predict high-grade (HG) histology of ccRCC, with results showing that MRI-based radiomic analysis was superior to tumour size in predicting HG histology (Dwivedi et al, 2021). Similarly, a study developed a machine learning model to predict 5-year mortality risk in patients with ccRCC using imaging data and constructed 8 different models (Nazari et al, 2021). The study found that the XGBoost model, which combined radiological characteristics with patient stage and grade, achieved the best performance (AUC = 0.97) among the eight models. This radiologically based classifier accurately predicts RCC survival, aiding in the prognosis of ccRCC patients.

In the realm of the US, a meta-analysis on the diagnostic value of contrast-enhanced US (CEUS) in renal clear cell carcinoma showed that CEUS offers high sensitivity and specificity, with excellent diagnostic accuracy (AUC between 0.9 and 1). CEUS, developed based on grayscale US, is more sensitive to microvessels in lesions and provides continuous, dynamic observations of blood perfusion in the lesion.

In this study, radiomics analysis was performed on CT images of kidney clear cell carcinoma. Five key radiomics features were ultimately selected based on the results from LASSO and the forward sequential method. The findings demonstrated that the logistic regression model exhibited high and stable diagnostic performance for patients with renal clear cell carcinoma. Machine learning not only integrates large volumes of imaging data but also deeply mines multidimensional imaging information to achieve accurate diagnosis and prediction (Heo et al, 2019). By integrating big data, machine learning can generate precise diagnostic and predictive insights from complex imaging data.

Two different supervised machine learning algorithms were employed to construct prediction models based on radiomics features. Among them, the logistic regression model showed superior and more stable diagnostic performance. This model is also widely used in clinical practice due to its ease of operation and suitability for constructing models with dichotomous variables (Christodoulou et al, 2019).

However, this study has several limitations, including its retrospective nature, small sample size, and lack of an external validation dataset. Future research should involve a large external validation set from multicenter studies to further develop and validate the proposed diagnostic model.

Conclusion

In conclusion, the machine learning-based radionics prediction model demonstrates excellent diagnostic efficiency, calibration, and clinical applicability for identifying patients with renal clear cell carcinoma. It holds promise as a valuable auxiliary tool for clinical decision-making.

Key Points

- A total of 44 radiomics features were utilized to develop the model.
- The logistic regression model demonstrated high diagnostic performance and stability in assessing clear cell renal cell carcinoma (ccRCC).
- Integrating clinical data with radiomics features improved the model's performance, achieving an area under the curve (AUC) of 0.969, with a sensitivity of 89.3% and a specificity of 95.2%.
- The calibration curve confirmed the model's high calibration accuracy and clinical utility.

Availability of Data and Materials

All experimental data included in this study can be obtained by contacting the first author if needed.

Author Contributions

GQ and HZ designed the research study. GQ, ZZD and HZ performed the research. GQ, ZZD and HZ analyzed the data. GQ drafted the manuscript. All authors contributed to the important editorial changes in the manuscript. All authors read and approved the final manuscript. All authors have participated sufficiently in the work and agreed to be accountable for all aspects of the work.

Ethics Approval and Consent to Participate

This study was conducted in accordance with the Declaration of Helsinki. The ethics committee of The First Affiliated Hospital of Chongqing Medical University waived the requirement for informed consent for this study.

Acknowledgement

Not applicable.

Funding

This research received no external funding.

Conflict of Interest

The authors declare no conflict of interest.

References

Avanzo M, Wei L, Stancanello J, Vallières M, Rao A, Morin O, et al. Machine and deep learning methods for radiomics. Medical Physics. 2020; 47: e185–e202. https://doi.org/10.1002/mp.13678

Binczyk F, Prazuch W, Bozek P, Polanska J. Radiomics and artificial intelligence in lung cancer screening. Translational Lung Cancer Research. 2021; 10: 1186–1199. https://doi.org/10.21037/tlcr-20-708

Bray F, Ferlay J, Soerjomataram I, Siegel RL, Torre LA, Jemal A. Global cancer statistics 2018: GLOBOCAN estimates of incidence and mortality worldwide for 36 cancers in 185 countries. CA: A Cancer Journal for Clinicians. 2018; 68: 394–424. https://doi.org/10.3322/caac.21492

Chen JY, Wang JZ, Zhang JH, Liu D, Zhang J, Xu XY, et al. Application of radiomics information captured from PET/CT and CT to predict therapeutic effect of stereotactic ablative radiotherapy in stage I non-small cell lung cancer. China Oncology. 2017; 27: 128–134.

Christodoulou E, Ma J, Collins GS, Steyerberg EW, Verbakel JY, Van Calster B. A systematic review shows no performance benefit of machine learning over logistic regression for clinical prediction models. Journal of Clinical Epidemiology. 2019; 110: 12–22. https://doi.org/10.1016/j.jclinepi.2019.02.004

Cohen HT, McGovern FJ. Renal-cell carcinoma. The New England Journal of Medicine. 2005; 353: 2477–2490. https://doi.org/10.1056/NEJMra043172

Dwivedi DK, Xi Y, Kapur P, Madhuranthakam AJ, Lewis MA, Udayakumar D, et al. Magnetic resonance imaging radiomics analyses for prediction of high-grade histology and necrosis in clear cell renal cell carcinoma: preliminary experience. Clinical Genitourinary Cancer. 2021; 19: 12–21.e1.

Frank I, Blute ML, Cheville JC, Lohse CM, Weaver AL, Zincke H. Solid renal tumors: an analysis of pathological features related to tumor size. The Journal of Urology. 2003; 170: 2217–2220. https://doi.org/10.1097/01.ju.0000095475.12515.5e

Heo J, Yoon JG, Park H, Kim YD, Nam HS, Heo JH. Machine Learning-Based Model for Prediction of Outcomes in Acute Stroke. Stroke. 2019; 50: 1263–1265. https://doi.org/10.1161/STROKEAHA.118.024293

Hsieh JJ, Purdue MP, Signoretti S, Swanton C, Albiges L, Schmidinger M, et al. Renal cell carcinoma. Nature Reviews. Disease Primers. 2017; 3: 17009. https://doi.org/10.1038/nrdp.2017.9

Jonasch E, Walker CL, Rathmell WK. Clear cell renal cell carcinoma ontogeny and mechanisms of lethality. Nature Reviews. Nephrology. 2021; 17: 245–261. https://doi.org/10.1038/s41581-020-00359-2

Lambin P, Rios-Velazquez E, Leijenaar R, Carvalho S, van Stiphout RGPM, Granton P, et al. Radiomics: extracting more information from medical images using advanced feature analysis. European Journal of Cancer. 2012; 48: 441–446. https://doi.org/10.1016/j.ejca.2011.11.036

Liu Z, Wang S, Dong D, Wei J, Fang C, Zhou X, et al. The applications of radiomics in precision diagnosis and treatment of oncology: Opportunities and Challenges. Theranostics. 2019; 9: 1303–1322. https://doi.org/10.7150/thno.30309

Liu ZJ, Yang F, Zhang B, Xu JX, Huang CC, Li WL, et al. Clinical value of unenhanced CT radiomic model in predicting WHO/ISUP grade of clear cell renal cell carcinoma. Modern Medicine Journal of China. 2022; 24: 57–61. (In Chinese)

Luo WS, Zhao LK, Liu TT, Zhang XL. The expression of Cripto-1 in renal clear cell carcinoma and its prognostic value. Chinese Journal of Laboratory Diagnosis. 2020; 24: 5. (In Chinese)

Lv D, Wu X, Wang M, Chen W, Yang S, Liu Y, et al. Functional Assessment of Four Novel Immune-Related Biomarkers in the Pathogenesis of Clear Cell Renal Cell Carcinoma. Frontiers in Cell and Developmental Biology. 2021; 9: 621618. https://doi.org/10.3389/fcell.2021.621618

Nazari M, Shiri I, Zaidi H. Radiomics-based machine learning model to predict risk of death within 5-years in clear cell renal cell carcinoma patients. Computers in Biology and Medicine. 2021; 129: 104135. https://doi.org/10.1016/j.compbiomed.2020.104135

Orlhac F, Nioche C, Klyuzhin I, Rahmim A, Buvat I. Radiomics in PET Imaging: A Practical Guide for Newcomers. PET Clinics. 2021; 16: 597–612. https://doi.org/10.1016/j.cpet.2021.06.007

Ran Y. Diagnostic performance of contrast-enhanced ultrasound for clear cell renal cell carcinoma: A meta-analysis [Master's Thesis]. Jilin University. 2022.

Shur JD, Doran SJ, Kumar S, Ap Dafydd D, Downey K, O'Connor JPB, et al. Radiomics in Oncology: A Practical Guide. Radiographics. 2021; 41: 1717–1732. https://doi.org/10.1148/rg.2021210037

Siegel RL, Miller KD, Jemal A. Cancer statistics, 2020. CA: A Cancer Journal for Clinicians. 2020; 70: 7–30. https://doi.org/10.3322/caac.21590

Song J, Shi J, Dong D, Fang M, Zhong W, Wang K, et al. A New Approach to Predict Progression-free Survival in Stage IV EGFR-mutant NSCLC Patients with EGFR-TKI Therapy. Clinical Cancer Research. 2018; 24: 3583–3592. https://doi.org/10.1158/1078-0432.CCR-17-2507

Su HF, Zhou GF, Xie CM, Cai PQ, Zhang R, Wu XL, et al. The rise and research progress of radiomics. National Medical Journal of China. 2015; 95: 553–557. (In Chinese)

Taha B, Boley D, Sun J, Chen CC. State of Radiomics in Glioblastoma. Neurosurgery. 2021; 89: 177–184. https://doi.org/10.1093/neuros/nyab124

Walsh S, de Jong EEC, van Timmeren JE, Ibrahim A, Compter I, Peerlings J, et al. Decision Support Systems in Oncology. JCO Clinical Cancer Informatics. 2019; 3: 1–9. https://doi.org/10.1200/CCI.18.00001

Wolff I, May M, Hoschke B, Zigeuner R, Cindolo L, Hutterer G, et al. Do we need new high-risk criteria for surgically treated renal cancer patients to improve the outcome of future clinical trials in the adjuvant setting? Results of a comprehensive analysis based on the multicenter CORONA database. European Journal of Surgical Oncology. 2016; 42: 744–750.

Xu K, Liu L, Li W, Sun X, Shen T, Pan F, et al. CT-Based Radiomics Signature for Preoperative Prediction of Coagulative Necrosis in Clear Cell Renal Cell Carcinoma. Korean Journal of Radiology. 2020; 21: 670–683. https://doi.org/10.3348/kjr.2019.0607

Xu K, Li J, Qin L, Liu J, Yang H, Dou G, et al. Decoding ecosystem heterogeneity and transcriptional regulation characteristics of multi-subtype renal cell carcinoma. Heliyon. 2024; 10: e33196. https://doi.org/10.1016/j.heliyon.2024.e33196